Manuscript Details

Manuscript number	VOLGEO_2020_250
Title	Impact of hydrothermal alteration processes on element mobility and potential environmental implications at the Sousaki solfataric field (Corinthia - Greece)
Article type	Research Paper

Abstract

Samples of efflorescences and encrustations of hydrothermal origin have been collected at Sousaki (Greece) and were analysed for their mineralogical (XRD) and chemical composition. Solutions obtained both from mineralization with HNO3 and from leaching with deionised water were analysed for major (ICP-OES), minor and trace metals (ICP-MS) and sulfate contents (IC). Results evidence the dependence of the chemical and mineralogical composition on micro-environmental conditions i.e. humidity, oxygen-rich or -poor environment, exposed or sheltered from meteoric agents. In fact, the presence of highly soluble sulfate minerals with elevated contents of many metals (e.g. Mg, Al, Fe, Mn, Cr, Ni, etc.) further underscores the important influence of hydrothermal activity on elements' mobility, whilst the sometimes very high concentrations in toxic elements like Al, Cr, Ni evidence also possible environmental impacts.

Keywords	Hydrothermal alteration products; sulfates; toxic metals; elements' mobility.

Corresponding Author	Sergio Calabrese
Order of Authors	Walter D'Alessandro, Sergio Calabrese, Sergio Bellomo, Lorenzo Brusca, Kyriaki Daskalopoulou, Lorenza Li Vigni, Luciana Randazzo, Konstantinos Kyriakopoulos
Suggested reviewers	Johan Varekamp, Giovanni Dinelli, Andri Stefansson, Franco Tassi

Submission Files Included in this PDF

File Name [File Type]

Coverletter.pdf [Cover Letter]

Fumarolic alteration 010720.doc [Manuscript File]

Fig1 bis.pdf [Figure]

Fig2.pdf [Figure]

Fig3.pdf [Figure]

Fig4.pdf [Figure]

Fig.5.pdf [Figure]

Fig6.pdf [Figure]

Table 1.docx [Table]

Table 2.docx [Table]

Table 3.docx [Table]

Table 4.docx [Table]

declaration-of-competing-interests.pdf [Conflict of Interest]

To view all the submission files, including those not included in the PDF, click on the manuscript title on your EVISE Homepage, then click 'Download zip file'.

Research Data Related to this Submission

There are no linked research data sets for this submission. The following reason is given:
Data will be made available on request

UNIVERSITÀ DEGLI STUDI DI PALERMO
Dipartimento di Scienze della Terra e del Mare (DiSTeM)
COD. FISC. 80023730825 ~ P.IVA 00605880822

Palermo, 08.07.2020

Dear Editor,

find as attachment the electronic source files related to the manuscript "*Impact of hydrothermal alteration processes on element mobility and potential environmental implications at the Sousaki solfataric field (Corinthia - Greece)*" by D'Alessandro et alii, submitted for publication in Journal of Volcanology and Geothermal Research.

The paper discusses the results of a multidisciplinary study on the chemical and mineralogical composition of efflorescences and encrustations of hydrothermal origin collected at Sousaki (Greece). The main aim of this work was to evaluate the mobility of the elements released by hydrothermal alteration and define the environmental pollution problems they were associated with.

The manuscript is original work, not published neither under consideration for publication elsewhere. All authors have seen the manuscript and they agree to its submission to this journal.

Yours sincerely
Sergio Calabrese

Please address further communications to:
Sergio Calabrese
Dipartimento di Scienze della Terra e del Mare (DiSTeM), Università degli Studi di Palermo
Via Archirafi, 36
90123 Palermo
Italy
Phone: +39 09123861648
e-mail: sergio.calabrese@unipa.it

Impact of hydrothermal alteration processes on element mobility and potential environmental implications at the Sousaki solfataric field (Corinthia - Greece)

W. D'Alessandro[1], S. Calabrese[1-2]*, S. Bellomo[1], L. Brusca[1], K. Daskalopoulou[3], L. Li Vigni[2], L. Randazzo[4], K. Kyriakopoulos[5]

1) Istituto Nazionale di Geofisica e Vulcanologia – Sezione di Palermo, Via U. La Malfa 153, 90146 Palermo, Italy

2) Università di Palermo, DiSTeM, via Archirafi 26, 90123 Palermo, Italy

3) GFZ German Research Centre for Geosciences, Physics of Earthquakes and Volcanoes, Helmholtzstraße 6/7, 14467, Potsdam, Germany

4) University of Calabria, Department of Biology, Ecology and Earth Science, DiBEST, via Pietro Bucci Cubo 12B, 87036, Arcavacata di Rende (CS), Italy

5) National and Kapodistrian University of Athens, Dept. of Geology and Geoenvironment, Panepistimioupolis, 157 84 Ano Ilissia, Greece

* corresponding author:

Abstract

Samples of efflorescences and encrustations of hydrothermal origin have been collected at Sousaki (Greece) and were analysed for their mineralogical (XRD) and chemical composition. Solutions obtained both from mineralization with HNO_3 and from leaching with deionised water were analysed for major (ICP-OES), minor and trace metals (ICP-MS) and sulfate contents (IC). Results evidence the dependence of the chemical and mineralogical composition on micro-environmental conditions i.e. humidity, oxygen-rich or -poor environment, exposed or sheltered from meteoric agents. In fact, the presence of highly soluble sulfate minerals with elevated contents of many metals (e.g. Mg, Al, Fe, Mn, Cr, Ni, etc.) further underscores the important influence of hydrothermal activity on elements' mobility, whilst the sometimes very high concentrations in toxic elements like Al, Cr, Ni evidence also possible environmental impacts.

Keywords: Hydrothermal alteration products; sulfates; toxic metals; elements' mobility.

1. Introduction

The mobility of elements in the exogenic cycle depends on the chemico-physical conditions that take place during weathering processes. While some of the elements displaying a high affinity for the aqueous phase are easily mobilized by water, other elements are retained in the soils that are forming as a consequence of weathering processes (Berner and Berner, 1996). These elements can be either retained in primary mineral phases, which are stable or metastable at the earth's surface, or incorporated in newly formed secondary minerals. Moreover, the mobility of some elements in the soils can be also severely limited by specific or non-specific adsorption onto organic matter; Al- and Fe-amorphous phases, phyllosilicates and Fe oxi-hydroxides.

Elements' mobility can be extremely favoured by a strongly acidic environment. Such conditions can be the result of natural processes like magmatic/geothermal degassing or even oxidation of sulfide minerals. These environments may reach extreme pH values as low as -3.6 (Nordstrom and Alpers, 1999). The consequent elements' mobilization has often a severe impact on the surrounding environment (Blowes et al, 2014). For instance, the Kawah Ijen crater lake in East Java (Indonesia) has a pH < 0.3, and is the feeding source of the extremely acidic and metal-contaminated river Banyupahit (Indonesian name for "bitter river"). The lake has a significant impact on the river's ecosystem as well as on a densely populated area downstream (Delmelle and Bernard, 2000; Löhr et al. 2005), where agricultural fields are irrigated with low pH waters (2.5 - 3.5) and whose metal concentrations exceed international quality guidelines, reaching extremely high values especially for Fe (up to 1600 mg/L) and Al (up to 3000 mg/L). Another important example can be found in the Iberian Pyrite Belt (SW Spain), which hosts one of the largest concentrations of massive sulfide deposits in the world, with about five millennia of mining history. Most of this mining district corresponds to the drainage basin of the Tinto and Odiel rivers. These, amongst the rivers affected by acid mine drainage worldwide, represent an extreme case of pollution with low pH values (between 1.0 and 3.0) and very high metal and metalloid concentrations (Cánovas et al, 2008). The metal discharges in the Huelva estuary (in which both rivers merge) have a regional impact due to the large metal inputs to the Mediterranean Sea (Elbaz-Poulichet et al, 2001).

Environmental studies of the processes generating metal-rich acid waters have highlighted the importance of metal-sulfate minerals forming upon evaporation,

oxidation and neutralization processes (Alpers et al, 2000; Cánovas et al., 2016; Grover et al., 2016). Some of these minerals are highly soluble and store metals and acidity only temporarily, whereas others are insoluble and improve water quality by removing metals from solutions (Cánovas et al., 2016). The formation of highly soluble efflorescent sulfate salts is highly favoured by dry climate conditions but may form also in areas where high rainfall occurs (Hammerstrom et al., 2005).

Metal-sulfate salts are common also around active crater lakes, fumaroles and acid hot springs. In these environments, H_2S oxidizes to elemental sulfur, which accumulates and further oxidates to form sulfuric acid. Then, the acid reacts with the surrounding bedrock leading to the formation of a variety of metal-sulfate minerals (Martin et al., 1999; Rodgers et al., 2000; Hall et al., 2003).

The study area of this paper, Sousaki, is a presently inactive volcanic area hosting a geothermal reservoir (Fytikas and Kavouridis, 1985). Geothermal activity, still recognizable by a series of low temperature gas manifestations, is responsible for the widespread alteration of the outcropping rocks in the area. The main manifestations are hosted within caves, whose walls are covered by alteration products present in the form of crusts and efflorescences (Kyriakopoulos et al, 1990; Balić-Žunić et al., 2016). The caves provide a sheltered, more or less stable environment, in which alteration processes can take place and where their products can persist. However, the same products can be found during dry periods also at strong degassing areas in open skies position.

This study presents the results of mineralogical and chemical analyses of the alteration products collected in the area. Leaching experiments were also performed both on the alteration products and on sediment samples collected along a creek, down flow the main gas manifestations, to get insights on the mobility of the elements released by hydrothermal alteration. Potential environmental impacts are also discussed.

2. Study area and methods

2.1. Geologic description of the area

Sousaki belongs to the westernmost sector of the Hellenic Volcanic Arc (Pe-Piper and Piper, 2002; Francalanci et al., 2005 - Fig.1), and is located about 65 km west of

Athens extending parallel to the northern coast of the Saronic Gulf for about 8 km with a width between 3 and 4 km inland. The region was affected by E-W and NE-SW extensional tectonics with the latter being of younger age and rather responsible for the volcanism as well as for the presence of several thermal manifestations (Kavouridis and Fytikas, 1988; Francalanci et al, 2005). Its activity spanned from mid- to late-Pliocene (age determinations range from 4.0 to 2.3 Ma – Collier and Dart, 1991; Fytikas et al, 1986), while the volcanic outcrops comprise lava flows and domes and subordinated tuffs of dacitic to rhyolithic composition (Pe-Piper and Hatzipanagiotou, 1997; Francalanci et al, 2005).

Besides volcanic rocks the following formations crop out in the area (IGME, 1985):

1. Quaternary sediments: consisting of unconsolidated material with sand and rounded and angular pebbles in the torrent beds, loose sandy – clayey material and alluvial sediments.
2. Neogene sediments: composed of marly conglomerates and marly sandstones.
3. Post-upper Cretaceous ophiolitic nappe: consisting of peridotites slightly serpentinized, serpentinites and bodies of basic composition.
4. Upper Triassic–lower Cretaceous limestones.

The hydrothermal activity of the volcanic area is evidenced by the presence of serpentinized peridotite and Late Pliocene – Pleistocene alluvial deposits presenting signs of extended silicification and argillification (D'Alessandro et al., 2006). Moreover, as Georgopoulos et al. (2018) highlighted, the degassing processes taking place in the area along with the acidic environment resulted in increased mobility of trace elements deriving from the ophiolite rock and the alluvial sediments. The presence of encrustations and efflorescences (Kyriakopoulos et al., 1990; Balić-Žunić et al., 2016) and secondary clays such as Cr – halloysite and Cr – smecite (Mitsis et al., 2018) support this statement.

2.2. Geothermal manifestations

Drilling exploration campaigns, performed during the late seventies, assessed the presence of a low enthalpy geothermal field, revealing two permeable formations at shallow depths (< 200 m) and one at deeper levels (500 – 1100 m). All geothermal waters are of Na-Cl type and display temperatures in the range of 50 – 80 °C and salinities in the range of 39 – 49 g/l (Fytikas et al. 1995). Widespread fumarolic

alteration and warm (38 – 42 °C) gas emissions are still recognizable (D'Alessandro et al. 2006; 2011). The geothermal reservoir and its degassing are likely controlled by active tectonic structures (Stiros, 1995). The surface manifestations seem to have been very stable in the last two centuries: several descriptions of the area made by eminent scientists since the 19th century are always very close to the present-day situation and also measured temperatures are in the same range (Fouqué, 1867; Ansted, 1873; Washington, 1924; von Leyden, 1940; Georgalas, 1962).

Extended argillification-silicification of the rocks characterises an area of about 200 × 700 m with widespread surface emanations called Thiochoma (Fig. 1c). The main vents are found at the bottom of two caves on the flank of a hill (Fig. 2a). The caves called "*big*" and "*small*" have the following dimensions (height × width × depth) 8×3×10 m and 4×1.5×4 m respectively. The emanating gases, being denser than atmospheric air, flow on the floors of the caves and eventually spill out from their mouth dispersing in the atmosphere after descending the flanks of the hill. This phenomenon can be seen when the atmospheric temperature is very low and the water vapour contained in the geothermal gases condenses, creating a thin fog layer at the contact between the cold atmospheric air and the warm geothermal gases.

The gas flux, being almost constant, with time creates a clear separation in the caves' atmosphere with an anoxic part on the floor, evidenced on the walls by a clear-cut line (Fig. 2b) separating the lower fumarolic alteration products, mainly composed of native sulfur and sulfides, from the upper more oxidizing portion composed mainly of sulfates (Kyriakopoulos et al. 1990; D'Alessandro et al. 2006).

Another smaller area displaying fresh hydrothermal alteration signs and characterized by lower gas emanation has been identified about 1 km to the east (Fig. 1c; D'Alessandro et al, 2006; 2011).

First data on the chemical composition of the gases were given by Fouqué (1867). The results obtained closely resemble recent analyses that point to a typical geothermal composition with CO_2 as the main component (>95%) and CH_4 (~8000 ppm) and H_2S (~1200 ppm) as minor components (Panichi et al, 2000; D'Alessandro et al. 2006; 2011; Daskalopoulou et al. 2018; 2019). It has been estimated that the two main gas manifestations of Sousaki release about 2 Mg/d of CO_2 and 2 kg/d of H_2S (D'Alessandro et al. 2006).

2.3. Climate of the area and rainfall data

The climate characterizing the area is of dry Mediterranean type with an average rainfall of less than 400 mm. The rainfall distribution displays great inter- and intra-annual variations, with 80% of the annual rainfall occurring between October and March, while rainfall is almost nil during July and August (Fig. 3). As a proxy of the rainfall at Sousaki, the meteorological station of the National Observatory of Athens at Thissio was used (www.noa.gr).

The efflorescence sample collection on 10 October 2004 was preceded by a very long dry spell period that started on 17 May and had a negligible rainfall activity on the 4th and 16th of June (totalling 0.4 mm). In 2008, the sediment sample collection on 9 October was preceded by a short but intense rainy period that took place from the 20th to the 24th of September, accounting for 40.8 mm rain height for the whole interval and peaking on the 21st (24 mm). This, followed a long dry spell lasting from the beginning of April (last rainfall 8th of April). In the latter period, two small episodes occurring on the 9th of June (6 mm) and on the 10th of August (1.7 mm) should not be considered significant.

2.4. Methods

Nine samples of fumarolic alteration products have been collected in October 2004 in three different places. Six of the samples were taken from the walls of the small cave. One of these (GR1) represents the wall's coating of the portion of the cave permanently saturated with the geothermal gases, while the remaining five (GR2 – GR6) were collected above the saturation surface at different heights (Fig. 2b).

One sample (AL1) was collected on the ground outside the caves at a distance of about 20 m from the entrance, well exposed to atmospheric agents. Two samples (AG1 and AG2) were collected at a smaller gas manifestation at the eastern area (Fig. 1), seeping from the ground at the base of a small overhanging cliff and thus, partially protected from atmospheric agents.

Samples were gently scraped from the walls with the polypropylene containers, in which they were stored. In the laboratory they were split into two aliquots for mineralogical and chemical analysis.

The sample for chemical analysis was firstly ground in an agate mortar and then further split into two aliquots. The first one was mineralised according to the following procedure. About 200 mg of the sample dried at 40 °C overnight were dissolved in a Teflon vessel with 6 ml HNO_3 (Merck Suprapur) and 4 ml milliQ water using a microwave oven. The solutions were heated for 5 minutes to a temperature of 170 °C, maintained for 5 minutes, and further heated at 180 °C for 10 minutes. Since the quantity of the collected sample was less, for GR3 and GR6 only about 100 mg were used. After cooling down, the solution was filtered (0.45 µm) and diluted with milliQ water up to 50 ml. A second oven-dried sample aliquot was leached with milliQ water with a sample/water ratio of about 0.01 for 4 hours with constant stirring. The solution was subsequently filtered through a 0.45 µm filter.

In October 2008, nine samples of superficial sediments were collected along the dry bed of the creek that crosses the hydrothermally altered area. The samples were collected along a distance of about 750 m, the first three within the area that displays the strongest diffuse release of hydrothermal gas from the soil (D'Alessandro et al., 2006) and close to the main gas manifestations. At the collection sites of samples S1 and S3, white encrustations were clearly visible and widespread.

Sediment samples were only leached with milliQ water, following the same procedure as for the efflorescence samples. All sediment samples were loose and had a fine texture (silt > 90 %) so they were not ground but only air-dried before leaching.

All obtained solutions were analysed for Al, As, B, Ba, Cd, Co, Cr, Cs, Cu, Fe, Li, Mn, Mo, Ni, Pb, Rb, Sb, Se, Sr, Th, U, V and Zn by ICP-MS (Agilent 7500 CE), Ca, K, Mg and Na by IC (Dionex DX120) or ICP-OES (Yobin Ivon Ultima 2) and SO_4 by IC (Dionex DX120). The analytical accuracy was checked analysing reference materials (SLRS-4 of the National Research Council of Canada and Spectrapure Standards SW1). Repeatability was always better then ± 10% for ICP-MS or ICP-OES and ± 5% for IC.

The mineralogical analysis was carried out by X-ray diffractometry at the National and Kapodistrian University of Athens.

Factor analysis (FA) was performed using the software SPSS (IBM) version 21 for windows.

3. Results

3.1. XRD analyses

Results of the X-ray diffraction analyses are displayed in Table 1. Based on their mineralogical composition, samples can be subdivided into three groups. Sample GR1, collected in the anoxic part of the cave, belongs to the first group and is composed almost exclusively of Native Sulfur. The second group comprises all the samples collected in the oxidized part of the cave and the two samples collected outside the cave in a relatively sheltered position. These samples are composed mainly of sulfates, with Calcium sulfate, both as Anhydrite and Gypsum, being ubiquitous. Other sulfates (Kieserite, Epsomite, Hexahydrite, Wairakite, Magnesiocopiapite, Alunogen), which are typical of hydrothermal environments, are also detected, whilst phases with different hydration states are found depending on local environmental conditions. Notably, phases with lower hydration state like Kieserite ($MgSO_4 \cdot H_2O$) and Anhydrite ($CaSO_4$) are found at the top of the cave, where both absolute and relative humidity are lower respect to the lower part of the cave. Also the samples collected outside the caves are probably exposed to environmental conditions leading to higher hydration states. Higher humidity conditions favour the formation of Hexahydrite ($MgSO_4 \cdot 6H_2O$) or Epsomite ($MgSO_4 \cdot 7H_2O$) and Gypsum ($CaSO_4 \cdot 2H_2O$). Sample AL1, which belongs to the last group, is mainly composed of Gypsum, but Calcite and Quartz were also identified.
Of the two sediments that were analysed by XRD, one (S1) was collected in the most affected by hydrothermal gas efflux area and showed the presence of abundant Gypsum, Clay Minerals (mainly Kaolinite) and Quartz, while the second (S9) was collected farthest from the hydrothermally affected area showing the presence of Calcite and Clay Minerals (Chlorite).

3.2. Chemical composition

3.2.1 Efflorescences and encrustations

Results of the chemical analyses are summarized in Table 2. Values obtained from HNO_3 mineralization can be considered as near-total concentrations because, generally, no visible solid residue was present after microwave acid digestion. The only exceptions were sample GR1 and AL1, where abundant yellow translucent and

scarce dark opaque residues were respectively observed. Some of the analysed elements (Cd, Sb, Se, Hg and Th) were always at or below the detection limit and were excluded from the table. Other elements (B, Ba, Cs, Cu, Li, Mo, Pb, Rb, U and V), with limited exceptions, display concentrations always below some tens of µg/g. Al, Ca, Fe and Mg display the highest variability, ranging from hundreds up to more than 100,000 µg/g. Cr and Ni show also elevated concentrations (thousands of µg/g). Samples obtained from leaching experiments display concentrations, which are the same as (within analytical error) or lower than those obtained with HNO_3 mineralization, indicating solubilities in water that vary from almost 100% down to 1% of the total concentration for the different elements in the different samples.

3.2.2. Factor analysis

The factor analysis was applied on both mineralised and leached samples and the results are shown in Table. 3.

Factor analysis performed on the chemical composition of the mineralised samples evidences four factors explaining 88.5% of the total variance of the dataset. The first factor (30.9 % variance) shows very high loadings (> 0.9) for Al, a series of transitional elements (Cr, Mn, Co, Cu and Zn) and U. Also Ni shows its highest loading on this factor (0.779). The highest loadings on the second factor (22.9 % of variance) are shown by Ca, K, Sr, Ba and Pb. In the third factor (18.4 % of variance) Na, Rb and Cs show very high loadings (> 0.95) while Li, Mg and Mo present their highest loadings (0.62 – 0.77). Finally, the fourth factor (16.3 % of variance) includes Fe, V and As with high loadings (> 0.87).

Factor analysis applied to the leachate samples gave similar results for the first two factors, while the third maintains a similarity only for two elements and the fourth shows a completely different behaviour. The first factor (34.9 % of variance) shows loadings (about 0.9) similar to those of the mineralised samples for Al, Cr, Mn, Co, Cu, Zn and U, while now Li and Na add to this factor with loadings of 0.67 and 0.75 respectively. In factor 2 (20.9 % of variance) Ca, Sr, Ba and Pb maintain high loadings (0.73-0.83), even though a bit lower than in the mineralised samples and B adds now to this factor with a loading of 0.78. In the third factor (20.2 % of variance) similar to the mineralised samples Rb, Mo and Ba maintain their high loadings (> 0.94), while As adds now to this factor (0.76). Finally, in the fourth factor (10.4 % of

variance) only Mg (0.94) and SO_4 (0.78) show high loadings. Potassium, V and Fe show, for the leachate samples, no high positive loadings and have instead strong negative loadings (K -0.66 on factor 3; V -0.70 and Fe -0.76 both on factor 2).

3.2.3. Sediment samples

The sediments' leaching solutions show a strong variation both in pH and Electric Conductivity (EC) along the sampling transect (Table 4 - Fig. 4). Samples collected in the hydrothermally affected area (S1 – S3) display the lowest pH values ranging from 6.13 to 7.98, while the remaining samples (S4 – S9) show higher and less scattered values (8.81 – 9.27). The alkaline pH of the less affected by hydrothermal input sediments can be attributed to the serpentinization processes of the ultramafic rocks of the area (Georgopoulos et al., 2018). On the contrary, EC shows an opposite pattern, with the highest values belonging to the first group (1173 – 2620 µS/cm) and the lowest to the second (90 – 431 µS/cm). The samples whose leachates have the highest EC values (S1 and S3) have displayed visible white incrustations probably made of soluble sulfates. As already seen (par. 3.1.1), the presence of gypsum has been ascertained in the sample S1.

4. Discussion

4.1. Relations between mineralogy, chemical composition and elements' mobility

In the study of the environmental impact of acid mine drainage waters, the mineralogical composition of efflorescences and incrustations has been sometimes compared to the chemistry of both the bulk composition and the leaching solutions (Cánovas et al., 2016; Carbone et al., 2013; Grover et al., 2016; Hammarstrom et al., 2005). Unfortunately, no universally accepted leaching protocol exists so far and despite the fact that leaching experiments are mostly made with deionised water, they differ in the water/solid ratio and in the leaching time. Nevertheless, as the majority of the minerals from efflorescences and incrustations are highly soluble, the results are generally comparable.

Based on the chemical composition, the samples of Sousaki can be subdivided into the same three groups as obtained from the mineralogical analysis. Only the sample

GR1 belongs to the first group (anoxic part of the cave) and displays very low concentrations for all elements with only few elements (Ca, Fe, K, Mg and Na) showing values higher than 100 µg/g. Loss of elements in the insoluble residue, likely composed exclusively of native sulfur, is improbable. The low concentrations are better explained by the fact that the lattice of native sulfur does not allow for extended substitutions and that the elements recognized in this group mainly derive from the debris falling from the upper walls of the cave.

The presence of highly soluble Al-, Fe- and Mg-sulfates in the samples of the second group justifies the high concentrations of these elements. The relatively high concentration of Ca derives from the ubiquitous presence of either anhydrite or gypsum. The presence of Nickel-hexahydrite found in the alteration products of Sousaki, identified in previous studies (Kyriakopoulos et al, 1990), explains the relatively elevated contents of Ni. Most of the analysed elements are found in the samples of this group in soluble form further evidencing their derivation from highly soluble mineral phases. In fact, all elements contained in high concentrations (Al, Ca. Fe and Mg) as well as many others (Co, Cr, Cs, Cu, Li, Mn, Ni, Rb, Sr, U and Zn) display average solubilities ranging from 70 to 94%. On the contrary, As, B, Ba, K, Mo, Na, Pb and V display lower average solubilities (4 – 56%). Except for As (up to 720 µg/g) and K (up to 50,000 µg/g), these low solubility elements display total concentrations rarely exceeding 10 µg/g.

In the last group (sample AL1) the great majority of the elements shows generally lower concentrations with respect to the samples of the previous group, displaying also a lower solubility (1 – 58%). Only a few elements (Ca, K, Ba, Sr and Pb) present concentrations up to two orders of magnitude higher than those of the previous group. Notably, these elements form sulfate phases with low (Ca and K) or very low (Ba, Pb and Sr) solubility. In this sample, which was exposed to atmospheric agents, low solubility phases become enriched because the most soluble phases have been removed by rainwater.

The factor analysis helps us in grouping the analysed elements with more or less homogeneous geochemical and mineralogical controls. These groups can be evidenced by comparing their loadings on the first three factors in Fig. 5. The associations that can be better recognised are the transitional elements (T in Fig. 5 – Cr, Mn, Co, Ni, Cu and Zn with the addition of Al and U), the less-soluble sulfate-forming elements (L in Fig. 5 – Ca, Sr, Ba and Pb with B and sometimes K), the iron-

related elements (I in Fig. 5 – Fe, V and As) and the alkaline elements (A in Fig. 5 – Li, Na and Cs, associated with Mo and sometimes with Mg, K and Rb).

The close association of Mn, Co, Ni, Cu and Zn can be easily explained by their tendency in substituting Fe^{II} or Mg in sulfates of the type $XSO_4 \cdot nH_2O$, where X is a bivalent cation (Nordstrom, 1999). As already mentioned, Nickel-Hexahydrite, which belongs to this group of minerals, has been previously identified in the efflorescences of Sousaki (Kyriakopoulos et al., 1990). The association with Al (sometimes substituted by Cr^{III}) may depend on the tendency of the above transitional metals to substitute bivalent cations (generally Fe^{II} or Mg) also in sulfates of the type $XY_2(SO_4)_4 \cdot nH_2O$, where X and Y are respectively bivalent and trivalent cations (Nordstrom, 1999). The association with U is more difficult to explain although the uranyl cation (UO^{2+}) sometimes substitutes for bivalent cations in more complex sulfate minerals (Nordstrom, 1999).

The association of Ca, Sr, Ba and Pb, as previously mentioned, can be explained by the low or very low solubility of the sulfate minerals they form.

The predisposition of V and As to be adsorbed on or incorporated in both Fe-oxihydroxides and Fe-sulfides may explain the close association of these two elements with iron (Blowes et al., 2014).

Finally, the alkaline elements show no (Li and Cs) or little (Na) affinity to sulfate minerals, which can explain their association (Nordstrom, 1999).

Mineralogical analyses of the present and previous studies (Kyriakopoulos et al., 1990; Balić-Žunić et al., 2016) evidenced the formation in such environmental conditions of a series of highly soluble sulfates. If we exclude Ca-sulfate phases, the main sulfate forming elements are Al, Fe and Mg. These elements derive from the fumarolic alteration of the outcropping ophiolitic rocks in a highly acidic environment (Kyriakopoulos et al., 1990; Balić-Žunić et al., 2016). In Fig. 6, the compositions of samples of the second group were plotted on a triangular diagram reporting the relative content of Al, Fe and Mg. On the same plot, the composition of the main sulfate minerals containing these elements is also shown. The position of the samples on the triangular plot conforms nicely with their mineralogical composition. In the samples GR2, GR4 and AG1, which plot close to the Mg vertex, Mg-sulfates (Kieserite or Hexahydrite) have been identified (Table 1). In the samples GR5 and AG2 that plot closer to the point representative of the Magnesiocopiapite composition, this mineral phase has actually been detected. Finally sample GR3,

which appears enriched in Al, is the only one (sample GR6 was not analysed by XRD) that contains detectable amounts of Alunogen.

Mg-sulfates are not so common on Earth with respect to Ca and Fe sulfates and to lesser degree Al-sulfates (Rodriguez et al. 2016). The recent exploration of Mars revealed that sulfates are diffuse alteration minerals and among them Mg-sulfates are very abundant (Ehlmann and Edwards, 2014). This has been related to a prevailingly basaltic composition of the Martian crust which is richer in Mg with respect to the Earth's crust (Chevrier and Mathé, 2007). Studying potential terrestrial analogues of Martian paleo-environments, Rodriguez et al. (2016) showed that Mg-sulfate oversaturation may be reached in low-pH, highly evaporated waters interacting with olivine-rich rocks. Such conditions can be easily reached at Sousaki where acid fluids interact with olivine-rich ultramafic rocks in a dry climate.

4.2. Elements distribution in the sediments along the creek

Possible receptors of the elements mobilised by highly acidic fluids are the surface waters. Rainwater dissolving the efflorescences and incrustations or acid drainage waters flow into creeks, rivers or lakes and are generally diluted by their freshwaters (Kimball, 1994; Cánovas et al., 2007). Notwithstanding the lowering in concentration and the change in environmental conditions (increased pH and Eh), other secondary minerals may precipitate impacting the composition of the sediments. Elements precipitated with or adsorbed on these new solid phases may be strongly retained or easily released to the hydrosphere as soon as the environmental conditions change again (Carbone et al., 2013).

At Sousaki, most of the very soluble elements deriving from the fumarolic alteration of the ophiolitic rocks, which are found in relatively high amounts in the efflorescence samples, display much lower values in the leachates of the sediment samples. This is probably due to the fact that about 2 weeks before a short and intense rainstorm impacted the study area (par. 2.3) dissolving and transporting away a significant part of the most soluble elements.

Nevertheless, the presence of soluble sulfates is confirmed by the good positive correlation between SO_4 concentrations and electric conductivity (Tab. 3). Also some of the elements deriving from the alteration of the ophiolitic rocks (Mg, Mn, Ni, Zn and Co) display a good correlation with sulfate pointing to the dissolution of soluble

sulfates containing these elements. A good positive correlation can also be noticed between SO_4 and Ca and Sr. The other analysed elements show very low or even no correlation with sulfate concentrations. Moreover, Al and Fe, which are an important component of the sulfate minerals of the efflorescences in the active hydrothermal manifestations, show no relations with SO_4 content in the sediment leachates. This could be explained either by the fact that Al- and Fe-sulfates form only in extremely acidic conditions (Blowes et al. 2014) that could not be met where hydrothermal fluxes are lower or by the fact that the mobility of Al and Fe is severely limited by the neutral or slightly basic and oxidizing environment in the creek's sediments.

Georgopoulos et al. (2018) analysed, among other samples, also the sediments of the same creek at Thiochoma. Although the leaching procedure is not the same as that applied in the present work, the measured pH values are comparable (7.6 – 9.3). Sulfate, Cr, Ni, Mn and Co in the leaching solutes, though similar, do not reach the highest values measured in the present work (except for Cr). This can be explained by the fact that their samplings were made during the rainy season and therefore the samples had probably lost part of their soluble fraction.

4.3. Environmental impact

When acid drainage waters are produced by oxidation of sulfide ore mining residues, many toxic elements may be mobilized and transported offsite at concentrations that can be of environmental concern (Alpers et al., 2000; Jerz and Rimstidt, 2003; Frau et al., 2015). Similarly, also the dissolution of the alteration products of fumarolic and solfataric fields may have a strong environmental impact (Fulignati et al., 2006). On the other hand, some toxic element tend to be trapped in insoluble secondary minerals that form also in such acidic environments. For example, Pb and Ba may be incorporated in low-solubility sulfates (Cánovas et al., 2016) or As, Se, V and Tl in clays (Mitsis et al., 2018).

At Sousaki, efflorescences and crusts within the cave are effectively sheltered from atmospheric agents and will be dissolved only rarely when intense rainfall produces infiltrations from the roof. But highly soluble alteration products form also outside the caves, especially within zones with high hydrothermal gas fluxes from the soil. Such zones cover an area of several thousands of m^2 (D'Alessandro et al., 2006) and are drained by a seasonal creek. The strong seasonality of rainfall in the area probably

produces a large peak in its water concentration for many harmful elements, when intense autumn precipitations dissolve the sulfates that formed during the long summer dry spell (Cánovas et al., 2007; Cidu et al., 2011). Furthermore, the recent climatic change will probably enhance possible environmental impact (Nordstrom, 2009). In the Mediterranean area, the precipitation regime shows a lengthening of the dry periods and at the same time an increase in number and severity of the extreme rainfall episodes (Brunetti et al., 2004). This would imply a higher probability of flash floods occurrence with strong peaks in toxic metal transport. Such flux of harmful elements could impact biota along the course of the creek and the marine environment close to its mouth which is about 1 km downstream. Although such impact has not been yet studied, it is worth noting that vegetation along the creek downstream of the hydrothermal manifestations is very stunted probably due to the bioavailability of the mobilized toxic elements.

Furthermore, Kelepertsis et al. (2001) and Georgopoulos et al. (2018) found anomalous enrichments in Ni, Co, Mn, Fe and Cr in the soils of the Sousaki area. The authors attributed such enrichment to the presence of the ophiolitic rocks. Indeed, such enrichments are typical of soils formed on these rocks (Quantin et al., 2008), but some of the anomalous values were found also in soils covering sedimentary formations. These are found along the creek downstream of the hydrothermal manifestations. Such enrichments could be due to the transport of the dissolved elements during flash floods, although transport of ophiolitic material deriving from physical weathering processes cannot be ruled out. Kelepertsis et al. (2001) found also an anomalous concentration of Ni (up to 163 µg/l) in the groundwater collected in the area of Sousaki. Notably, the highest values were all found in the waters collected in three wells very close to the creek. Furthermore, anomalous concentrations of Cr and Ni, which the authors attributed to a geogenic origin, have been found both in seawater and marine sediments in coastal and offshore stations in the Saronikos Gulf close to the mouth of the creek (Paraskevopoulou et al., 2010).

5. Conclusions

A multidisciplinary study on efflorescences and incrustations of hydrothermal origin, as well as sediment samples, was carried out in the area of Sousaki (Greece). The aim

of this work was to evaluate the mobility of the elements released by hydrothermal alteration and define the environmental pollution problems they were associated with.

Chemical and mineralogical compositions of efflorescences and incrustations are strongly dependent on both the ultramafic composition of the rocks characterizing the study area and the microenvironmental conditions of the sampling site. The former factor explains the strong enrichment in elements like Mg, Fe, Ni and Cr. The sulfate minerals formed by the fumarolic activity are sometimes very soluble. Their persistence can be explained by their growth in sites sheltered from meteoric precipitations and/or during the long dry periods that characterise the local climate. Less soluble sulfates may accumulate in sites subject to leaching by rainwater. Elemental sulfur was found only at sites where anoxic conditions are maintained by the flux of fumarolic gases.

The strong fumarolic alteration temporarily stores high quantities of many elements among which some are toxic (e.g. Ni, Cr, etc.). The first flushes after long dry periods may transport high levels of these harmful toxic contaminants. At highest risk is the biota along the creek draining the study area and in the marine environment close to the mouth.

Results deriving from this work could be of great importance for designing adequate contamination reduction strategies as well as for general geochemical implications.

Acknowledgements

We acknowledge the help of Claudio Bruno, Giuseppe Casà and Fernando Plicanti in the field and in the laboratory.

References

Alpers, C.N., Jambor, J.L., Nordstrom, D.K., (eds.) 2000. Sulfate Minerals – Crystallography, Geochemistry and Environmental Significance. Rev. Min. Geochem. 40, 608pp.

Ansted, T., 1873. On solfataras and deposits of sulphur at Kalamaki, near the Isthmus of Korinth. Q. J. Geol. Soc. 29, 360-363.

Balić-Žunić, T., Garavelli, A., Jakobsson, S.P., Jonasson, K., Katerinopoulos, A., Kyriakopoulos, K., Acquafredda, P., 2016. Fumarolic Minerals: An Overview of

Active European Volcanoes. In: Updates in Volcanology - From Volcano Modelling to Volcano Geology (Nemeth K. ed), IntechOpen, DOI: 10.5772/64129.

Berner, E.K., Berner, R.A., 1996. Global environment: Water, air, and geochemical cycles. Prentice-Hall.

Blowes, D.W., Ptacek, C.J., Jambor, J.L., Weisener, C.G., Paktunc, D., Gould, W.D., Johnson, D.B., 2014. 11.5 - The Geochemistry of Acid Mine Drainage. In: Holland, H.D., Turekian, K.K., (eds.) Treatise on Geochemistry (2nd Edition) Vol. 11, 131-190.

Brunetti, M., Buffoni, L., Mangianti, F., Maugeri, M., Nanni, T., 2004. Temperature, precipitation and extreme events during the last century in Italy. Glob. Planet. Changes, 40, 141-149.

Cánovas, C.R., Olias, M., Nieto, J.M., Sarmiento, A.M., Ceron, J.R., 2007. Hydrogeochemical characteristics of the Tinto and Odiel Rivers (SW Spain). Factors controlling metal contents. Sci. Total Environ., 373 363–382

Cánovas, C.R., Hubbard, C.G., Olias, M., Nieto, J.M., Black, S., Coleman, M.L., 2008. Hydrochemical variations and contaminant load in the Rio Tinto (Spain) during flood events. J. Hydrol. 350, 25–40.

Cánovas, C.R., Macías, F., Pérez-López, R., 2016. Metal and acidity fluxes controlled by precipitation/dissolution cycles of sulfate salts in an anthropogenic mine aquifer. J. Contam. Hydrol. 188, 29–43

Carbone, C., Dinelli, E., Marescotti, P., Gasparotto, G., Lucchetti, G., 2013. The role of AMD secondary minerals in controlling environmental pollution: Indications from bulk leaching tests. J. Geochem. Explor. 132, 188-200

Chevrier, V., Mathé, P.E. (2007) Mineralogy and evolution of the surface of Mars: a review. Plan. Space Sci. 55, 289–314

Cidu, R., Frau, F., Da Pelo, S., 2011. Drainage at Abandoned Mine Sites: Natural attenuation of contaminants in different seasons. Mine Water and the Environment 30, 113–126

Collier, R.E.L., Dart, C.J., 1991. Neogene to Quaternary rifting, sedimentation and uplift in the Corinth Basin, Greece. J. Geol. Soc. London 148, 1049-1065.

D'Alessandro, W., Brusca, L., Kyriakopoulos, K., Rotolo, S., Michas, G., Minio, M., Papadakis, G., 2006. Diffuse and focussed carbon dioxide and methane emissions from the Sousaki geothermal system, Greece. Geophys. Res. Lett. 33, L05307.

D'Alessandro, W., Brusca, L., Kyriakopoulos, K., Martelli, M., Michas, G., Papadakis, G., Salerno, F., 2011. Diffuse hydrothermal methane output and evidence of methanotrophic activity within the soils at Sousaki (Greece). Geofluids, 11, 97–107

Daskalopoulou, K., Calabrese, S., Grassa, F., Kyriakopoulos, K., Parello, F., Tassi, F., D'Alessandro, W., 2018. Origin of methane and light hydrocarbons in natural fluid emissions: a key study from Greece. Chem. Geol. 479, 286-301

Daskalopoulou, K., Calabrese, S., Gagliano, A.L., D'Alessandro, W., 2019. Estimation of the geogenic carbon degassing of Greece. Appl. Geochem. 106, 60-74

Delmelle, P., Bernard, A., 2000. Downstream composition changes of acidic volcanic waters discharged into the Banyupahit stream, Ijen caldera, Indonesia. J. Volcanol. Geotherm. Res. 97, 55–75.

Ehlmann, B.L., Edwards, C.S. (2014) Mineralogy of the Martian surface. Ann. Rev. Earth Plan. Sci. 42, 291–315

Elbaz-Poulichet, F., Braungardt, C., Achterberg, E., Morley, N., Cossa, D., Beckers, J., Nomerange, P., Cruzado, A., Leblanc, M., 2001. Metal biogeochemistry in the Tinto-Odiel rivers (Southern Spain) and in the Gulf of Cadiz: a synthesis of the results of the TOROS project. Contin. Shelf Res. 21, 1961–1973.

Fouquè, F., 1867. Les anciens volcans de la Grece. Revue des deux Mondes 67, 470-490.

Francalanci, L., Vougioukalakis, G.E., Perini, G., Manetti, P., 2005. A west-east traverse along the magmatism of the south Aegean volcanic arc in the light of volcanological, chemical and isotope data. In: The south Aegean active volcanic arc (Fytikas M., Vougioukalakis G.E. eds.) – Develop. Volcanol. 7, 65-111.

Frau, F., Medas, D., Da Pelo, S., Wanty, R.B., Cidu, R., 2015. Environmental effects on the aquatic system and metal discharge to the Mediterranean Sea from a near-neutral zinc-ferrous sulfate mine drainage. Wat. Air Soil Pollut. 226, 55

Fytikas, M., Kavouridis, Th., 1985. Geothermal area of Sousaki-Loutraki. In: Romijn, E., Groba, E., Luttig, G., Fiedler, K., Laugier, R., Lohnert, E., Karagunis, C. (Eds.), Geothermics, Thermal-Mineral Waters and Hydrogeology. Theophrastus Publications, Athens, pp. 19–34.

Fytikas, M., Giuliani, O., Innocenti, F., Kolios, N., Manetti, P., Mazzuoli, R., 1986. The Plio-Quaternary volcanism of Saronikos area (western part of the active Aegean volcanic Arc). Ann. Geol. Pays Hell. 33, 23-45.

Fytikas, M., Dalambakis, P., Karkoulias, V., Mendrinos, D., 1995. Geothermal exploration and development activities in Greece during 1990–1994. Proc. World Geotherm. Congr. Rome 1995.

Georgalas, G.C., 1962. Catalogue of the active volcanoes and solfatara fields of Greece. In: Catalogue of the active volcanoes of the World, International Association of Volcanology (pp. 1–40).

Georgopoulos, G., Mitsis I., Argyraki A., Stamatakis, M., 2018. Environmental availability of ultramafic rock derived trace elements in the fumarolic - geothermal field of Soussaki area, Greece. Appl. Geochem. 92, 9–18

Grover, B.P.C., Johnson, R.H., Billing, D.G., Weiersbye, I.M.G., Tutu, H., 2016. Mineralogy and geochemistry of efflorescent minerals on mine tailings and their potential impact on water chemistry. Environ. Sci. Pollut. Res. 23, 7338–7348

Hall, A.J., Fallick, A.E., Perdikatsis, V., Photos-Jones, E. 2003. A model for the origin of Al-rich efflorescences near fumaroles, Melos, Greece: enhanced weathering in a geothermal setting. Mineral. Mag. 67 (2), 363–379.

Hammarstrom, J.M., Seal, R.R. II, Meier, A.L., Kornfeld, J.M., 2005 Secondary sulfate minerals associated with acid drainage in the eastern US: Recycling of metals and acidity in surficial environments. Chem. Geol., 215(1), 407-431

IGME, 1985. Geological map of Greece 1/50,000 - Sofikon sheet. Institute of Geology and Mineral Exploration, Athens.

Jambor, J.L., Nordstrom, D.K., Alpers, C.N., 2000. Metal-sulfate salts from sulfide mineral oxidation. In: Alpers C.N., Jambor J.L., Nordstrom D.K. (eds.) Sulfate Minerals: Crystallography, Geochemistry, and Environmental Significance. Rev. Mineral. Geochem. 40, 303–350.

Jerz, J.K., Rimstidt, J.D., 2003. Efflorescent iron sulfate minerals: Paragenesis, relative stability, and environmental impact. Am. Mineral. 88, 1919–1932.

Kavouridis, Th., Fytikas, M., 1988. Geothermal investigations in the area of Sousaki: Technical Report (In Greek), Institute of Geological and Mineral Exploration (IGME), Greece.

Kelepertsis, A., Alexakis, D., Kita, I., 2001. Environmental geochemistry of soils and waters of Susaki area, Korinthos, Greece. Environ. Geochem. Health 23, 117-135.

Kimball, B.A., 1994. Seasonal variation in metal concentrations in a stream affected by acid mine drainage, St. Kevin Gulch, Colorado. In: Filipek L.H., Plumlee G.S., eds. The environmental geochemistry of mineral deposits, Part B: case studies and research topics. Rev. Econ. Geol., 6B, 467–477.

Kyriakopoulos, K., Kanakis-Sotiriou, R., Stamatakis, M.G., 1990. The authigenic minerals formed from volcanic emanations at Soussaki, W. Attica peninsula, Greece. Can. Mineral. 28, 363-368.

Löhr, A.J., Bogaard, T.A., Heikens, A., Hendriks, M.R., Sumarti, S., Van Bergen, M.J., Van Gestel, C.A.M., Van Straalen, N.M., Vroon, P.Z., Widianarko, B., 2005. Natural Pollution Caused by the Extremely Acidic Crater Lake Kawah Ijen, East Java, Indonesia. Environ. Sci. Pollut. Res. 12, 89–95.

Martin, R., Rodgers, K.A., Browne, P.R.L., 1999. The nature and significance of sulphate-rich, aluminous efflorescences from the Te Kopia geothermal field, Taupo Volcanic Zone, New Zealand. Min. Mag. 63, 413-419.

Mitsis, I., Godelitsas, A., Göttlicher, J., Steininger, R., Gamaletsos, P.N., Perraki, M., Abad-Ortega, M.M., Stamatakis, M., 2018. Chromium-bearing clays in altered ophiolitic rocks from Crommyonia (Soussaki) volcanic area, Attica, Greece. Appl. Clay Sci., 162, 362–374

Nordstrom, D.K., 1999. Sulfates, In: Encyclopedia of Environmental Science (Alexander D.E., Fairbridge R.W., eds.) Kluwer Academic Publisher, 580-585

Nordstrom, D.K., 2009. Acid rock drainage and climate change. J. Geochem. Explor. 100, 97–104.

Nordstrom, D.K., Alpers, C.N., 1999. Negative pH, efflorescent mineralogy, and consequences for environmental restoration at the Iron Mountain Superfund site, California. Proc. Natl. Acad. Sci., 96 (7), 3455-3462

Panichi, C., La Ruffa, G., Kavouridis, T., Leontiadis, J., Leonis, C., Liberopoulou, V., Dotsika, E., 2000. Geochemical assessment of the thermal fluids emerging along the Aegean Volcanic Arc (Greece). Proc. World Geotherm. Congr. Kyushu - Tohoku, Japan, May 28 - June 10, 2000, 1565-1570.

Paraskevopoulou, V., Triantafyllaki, S., Giannikopoulos, N., Dassenakis, M., 2010. Dissolved and particulate nickel distribution in a coastal marine area affected by

geochemical and industrial processes. Fresenius Environmental Bulletin 19(9), 1833-1840

Pe-Piper, G., Hatzipanagiotou, K., 1997. The Pliocene volcanic rocks of Crommyonia, W. Greece and their implications for the early evolution of the South Aegean arc. Geol. Mag. 134, 55-66.

Pe-Piper, G., Piper, D.J.W., 2002. The igneous rocks of Greece. Bornträger, Berlin.

Quantin, C., Ettler, V., Garnier, J., Sebek, O., 2008. Sources and extractibility of chromium and nickel in soil profiles developed on Czech serpentinites. C. R. Geosci. 340, 872–882.

Rodgers, K.A., Hamlin, K.A., Browne, P.R.L., Campbell, K.A., Martin, R., 2000. The steam condensate alteration mineralogy of Ruatapu cave, Orakei Korako geothermal field, Taupo Volcanic Zone, New Zealand. Min. Mag. 64, 125-142.

Rodríguez, A., Varekamp, J.C., van Bergen, M.J., Kading, T.J., Oonk, P., Gammons, C.H. Gilmore, M. (2016) Acid Rivers and Lakes at Caviahue-Copahue Volcano as Potential Terrestrial Analogues for Aqueous Paleo-Environments on Mars. In: Tassi F., Vaselli O., Caselli A. (eds) Copahue Volcano. Active Volcanoes of the World. Springer, Berlin, Heidelberg

Stiros, S.C., 1995. The 1953 seismic surface fault: implications for the modelling of Sousaki (Corinth area, Greece) geothermal field. J. Geodyn. 20, 167-180.

von Leyden, R., 1940. Der Vulkanismus des Golfes von Ägina und seine Beziehungen zur Tektonik. Vulkaninstitut Immanuel Friedländer No 1, Zürich.

Washington, H.S., 1924. Notes on the Solfatara of Sousaki (Greece), a recent eruption at Methana (Greece), and recent Maccalube at Vulcano. J. Geol. 32, 460-462.

Tables

Table 1. Results of the XRD analysis

Sample	Mineral phases
AL1	Gypsum
GR1	Native Sulfur
GR2	Kieserite, Anhydrite
GR3	Anhydrite, Cristobalite, Alunogen
GR4	Anhydrite, Hexahydrite, Wairakite
GR5	Magnesiocopiapite
AG1	Epsomite, Gypsum
AG2	Hexahydrite, Gypsum, Magnesiocopiapite
S1	Gypsum, Clay minerals, Quartz
S9	Calcite, Clay minerals

Table 2 – Results of the chemical analyses of the efflorescences

Mineralization																							
	Li	B	Na	Mg	Al	K	Ca	V	Cr	Mn	Fe	Co	Ni	Cu	Zn	As	Rb	Sr	Mo	Cs	Ba	Pb	U	SO_4
	µg/g																							
AL1	0.53	2.97	723	895	641	50000	175000	2.72	122	4.92	901	1.36	19.0	0.62	4.64	10.5	2.85	198	0.43	2.01	117	15.3	0.03	399000
GR1	0.12	9.79	283	1310	60	12000	4120	0.11	7.19	5.20	177	1.39	30.8	1.16	21.8	3.58	0.02	1.80	0.20	0.01	1.02	1.44	< 0.02	476000
GR2	8.70	6.69	2040	134000	2510	17000	15600	3.86	319	439	16800	165	3390	13.1	38.8	119	16.6	59.0	1.53	9.98	1.52	0.79	0.82	946000
GR3	5.47	10.9	674	90500	3080	23200	25300	1.75	136	525	2680	144	2780	8.98	25.2	20.8	1.32	51.4	< 0.02	1.42	2.25	0.52	1.49	952000
GR4	2.19	4.76	632	52900	43000	26500	21200	2.55	2140	1070	10200	431	6940	27.9	61.9	16.0	0.81	27.5	0.19	1.20	2.06	0.27	1.43	926000
GR5	7.83	2.98	504	43600	22000	21500	3990	19.8	3680	937	99000	235	7230	16.7	41.9	680	2.88	4.59	1.07	3.72	0.01	0.01	1.47	919000
GR6	8.92	6.55	788	40500	40700	25100	1580	2.67	5490	2740	6480	488	6550	180	87.2	43.1	2.34	10.9	0.30	3.09	0.29	0.41	12.7	982000
AG1	3.03	1.95	571	147000	244	22700	20100	0.83	37.4	154	1220	60.4	2170	2.28	6.35	8.12	0.43	80.2	0.16	0.67	1.80	0.35	0.11	914000
AG2	0.95	2.28	145	1180	5610	10200	479	18.6	1510	519	101000	141	2850	5.90	25.9	230	1.77	34.9	0.73	1.94	0.49	0.13	0.29	926000

Leaching																							
	Li	B	Na	Mg	Al	K	Ca	V	Cr	Mn	Fe	Co	Ni	Cu	Zn	As	Rb	Sr	Mo	Cs	Ba	Pb	U	SO_4
	µg/g																							
AL1	0.14	1.72	320	422	34.1	10800	42000	0.03	4.74	1.08	28.4	0.38	5.34	0.60	1.46	0.40	0.24	98.8	0.16	0.17	1.33	3.18	0.01	99600
GR1	0.09	0.68	169	121	51.6	6320	663	0.06	6.08	4.73	155	1.33	30.6	0.06	4.71	1.10	0.16	1.82	< 0.03	0.11	0.08	0.34	< 0.03	13000
GR2	9.88	0.97	439	26700	3930	3140	2630	3.99	281	421	16500	149	3340	12.1	35.9	86.6	18.6	59.8	1.17	11.4	1.09	0.67	0.85	620000
GR3	7.42	0.71	579	113000	5570	12300	34200	0.20	137	625	2160	164	3420	9.16	18.3	1.47	1.56	67.8	< 0.05	1.60	0.63	0.29	1.79	515000
GR4	1.70	0.24	237	35300	41600	10900	13900	1.80	1635	800	8250	333	5480	18.5	42.6	10.7	0.67	23.5	< 0.06	0.87	0.59	0.12	1.03	489000
GR5	7.87	< 0.04	403	34600	24300	10800	2640	4.04	2952	753	61800	197	6220	13.1	34.4	53.3	2.75	4.67	< 0.04	3.53	< 0.04	0.02	1.24	458000
GR6	10.1	< 0.04	669	44800	47700	9890	2900	2.04	5144	2530	7080	447	6220	179	81.0	21.6	2.58	12.4	0.15	3.25	0.10	0.40	12.8	476000
AG1	2.82	< 0.04	236	113000	195	6470	12300	0.08	20.6	137	872	52.9	2020	1.87	5.35	1.23	0.35	65.2	< 0.04	0.50	0.53	0.21	0.09	547000
AG2	0.92	< 0.04	114	40600	5370	6100	805	16.9	1174	386	78700	119	2360	5.14	21.6	99.6	1.60	36.6	0.51	1.63	0.22	0.04	0.25	508000

Se, Cd, Sb, Hg and Th were always below detection limit.

Table 3 – Factor analysis

mineralized	F1	F2	F3	F4
Li	0.562	-0.250	0.675	0.069
B	0.004	-0.324	0.045	-0.634
Na	0.063	0.095	0.956	-0.241
Mg	-0.108	-0.324	0.616	-0.334
Al	0.903	-0.094	-0.130	0.080
K	0.135	0.925	-0.031	-0.128
Ca	-0.225	0.962	-0.030	-0.076
V	0.026	-0.180	-0.029	0.966
Cr	0.919	-0.106	-0.066	0.337
Mn	0.978	-0.137	0.020	-0.004
Fe	-0.005	-0.261	-0.044	0.948
Co	0.926	-0.217	0.063	0.029
Ni	0.779	-0.320	0.142	0.345
Cu	0.916	-0.015	0.013	-0.183
Zn	0.925	-0.258	0.117	-0.015
As	0.093	-0.194	0.130	0.886
Rb	-0.072	0.018	0.965	0.037
Sr	-0.350	0.874	0.112	-0.118
Mo	-0.076	-0.039	0.772	0.571
Cs	0.093	-0.011	0.963	0.169
Ba	-0.194	0.976	-0.065	0.001
Pb	-0.217	0.967	-0.065	-0.038
U	0.906	-0.025	0.017	-0.189
SO_4	0.443	-0.620	0.329	0.146

leached	F1	F2	F3	F4
Li	0.669	0.098	0.483	0.410
B	-0.335	0.777	0.211	-0.440
Na	0.746	0.450	0.157	0.290
Mg	-0.028	0.085	-0.193	0.938
Al	0.876	-0.200	-0.187	0.014
K	0.351	0.323	-0.659	0.141
Ca	-0.231	0.826	-0.299	0.098
V	-0.148	-0.697	0.347	-0.029
Cr	0.911	-0.318	-0.080	-0.056
Mn	0.973	-0.093	-0.024	0.086
Fe	-0.082	-0.755	0.243	0.028
Co	0.911	-0.163	0.006	0.204
Ni	0.777	-0.285	0.066	0.396
Cu	0.925	-0.005	-0.028	-0.082
Zn	0.947	-0.192	0.196	0.057
As	-0.032	-0.561	0.758	-0.001
Rb	0.084	0.096	0.957	0.065
Sr	-0.440	0.737	0.201	0.190
Mo	-0.080	-0.027	0.981	-0.072
Cs	0.226	0.024	0.937	0.106
Ba	-0.321	0.780	0.389	-0.049
Pb	-0.190	0.731	0.029	-0.519
U	0.929	0.027	-0.042	-0.028
SO_4	0.270	-0.215	0.444	0.783

Table 4 – Physico-chemical parameters measured in the leachate solutions of the sediment samples and results of the chemical analyses

Sample	distance	pH	E.C.	Li	B	Na	Mg	Al	K	Ca	V	Cr	Mn	Fe	Co	Ni	Cu	Zn	As	Rb	Sr	Mo	Cs	Ba	Pb	U	SO_4
	m		µS/cm	µg/g																							
S1	0	6.13	2620	0.65	0.76	168	40500	0.09	174	22200	0.01	0.15	197	79.0	8.10	195	0.07	0.83	0.06	0.26	40.7	0.04	0.01	0.89	<0.01	<0.01	193000
S2	51	7.98	1173	0.12	0.50	21.6	649	0.22	57.5	22400	0.01	0.03	31.4	0.43	0.17	1.89	0.08	0.31	0.49	0.22	33.4	0.13	0.02	0.59	0.01	<0.01	54000
S3	81	7.38	1690	0.61	0.74	30.0	12100	1.10	37.2	24500	0.01	0.01	111	0.35	1.62	47.0	0.01	0.35	0.10	0.20	50.4	0.09	0.01	0.61	<0.01	0.02	106000
S4	100	8.87	431	0.54	0.75	232	846	0.86	153	6260	0.05	<0.01	3.47	0.62	0.04	0.97	0.04	<0.01	0.26	0.67	16.1	0.06	0.07	0.54	<0.01	<0.01	17100
S5	159	8.96	158	0.23	0.35	37.6	189	2.34	96.5	1600	0.09	0.02	0.37	1.36	0.00	0.11	0.05	0.43	0.27	0.42	3.9	0.05	0.04	0.49	<0.01	<0.01	3870
S6	215	9.10	120	0.13	0.33	36.4	201	1.35	85.2	1460	0.14	0.01	0.11	1.32	0.00	0.06	0.04	0.01	0.15	0.27	3.8	0.05	0.02	0.37	<0.01	<0.01	3500
S7	339	8.81	295	0.08	0.23	11.0	381	0.20	75.0	4250	0.06	0.01	1.10	0.35	0.01	0.18	0.02	0.05	0.35	0.18	6.6	0.05	0.01	0.41	<0.01	<0.01	10900
S8	436	9.15	118	0.18	0.33	40.2	126	4.57	96.7	858	0.14	0.01	0.13	2.71	0.00	0.11	0.05	<0.01	0.26	0.31	2.3	0.04	0.02	0.46	<0.01	<0.01	141
S9	753	9.27	90	0.24	0.82	54.7	170	11.1	217	677	0.41	0.07	0.24	16.5	0.02	0.54	0.23	<0.01	0.52	0.33	2.0	0.04	0.03	0.47	0.01	0.01	944

distance = progressive distance from the first sampling site along the creek. E.C. = Electric Conductivity. Se, Cd, Sb, Hg and Th were always below detection limit.

Captions

Fig. 1 – (a) Location of the Sousaki geothermal system with respect to the south Aegean volcanic arc (volcanoes with historical activity are evidenced with a red triangle); (b) Area of the Isthmus of Corinth; (c) Study area with sampling points. Symbols as follows: Orange circle = main gas manifestations (samples GR 1 - 6 have been collected inside the small cave and sample AL1 has been collected outside); Green square = minor alteration (samples AG1 and AG2); Blue triangles sediment samples (Sampling sequence from S1 to S9 down flow from north to south).

Fig. 2 – (a) Picture of the main gas manifestations area. White arrows indicate the two caves (Big cave on the left, small cave on the right), the black arrow shows the sampling site of sample AL1. A red oval evidences one of the authors for scale. (b) Inside view of the small cave. Red arrows evidence the clear-cut separation of the lower anoxic part of the cave. Sample GR 1 has been collected below this line while samples GR 2 – 6 have been collected above. The white arrow shows the flow direction of the fumarolic gases which spill out of the cave through a threshold which is about 40 cm wide as indicated by the black arrows. Close-up view of efflorescences (c) and incrustations (d) inside the small cave. The scale shown in (c) is about the same in both close-up views.

Fig. 3 – Rainfall data (in mm) measured by National Observatory of Athens at the meteorological station of Thissio. Data of the years 2004 and 2008 are compared to the mean values of the period 1961-1990.

Fig. 4 – Variations of Electric Conductivity and pH in the leaching solutions of the sediment's samples collected along the creek.

Fig. 5 – Binary plots comparing the loadings of the elements: factor 1 vs. factor 2 (a and c) and factor 1 vs. factor 3 (b and d) in mineralized (a and b) and leachate (c and d) solutions. The identified elements' association has been evidenced with areas of different colours: T = Cr, Mn, Co, Ni, Cu, Zn, Al and U; L = Ca, Sr, Ba and Pb; I = Fe, V and As; A = Li, Na, Cs and Mo.

Fig. 6 – Al-Fe-Mg triangular plot of the chemical composition of the efflorescence samples (on weight basis). The chemical composition of the main sulfate minerals containing these elements are also plotted. Pickeringite [$MgAl_2(SO_4)_4{\cdot}22(H_2O)$]; Alunogen [$Al_2(SO_4)_3{\cdot}17(H_2O)$]; Halotrichite [$Fe^{II}Al_2(SO_4)_4{\cdot}22(H_2O)$]; Copiapite [$Fe^{II}Fe^{III}_4(SO_4)_6(OH)_2{\cdot}20(H_2O)$]; Aluminocopiapite [$Al_{2/3}Fe^{III}_4(SO_4)_6(OH)_2{\cdot}20(H_2O)$]; Magnesiocopiapite [$MgFe^{III}_4(SO_4)_6(OH)_2{\cdot}20(H_2O)$].

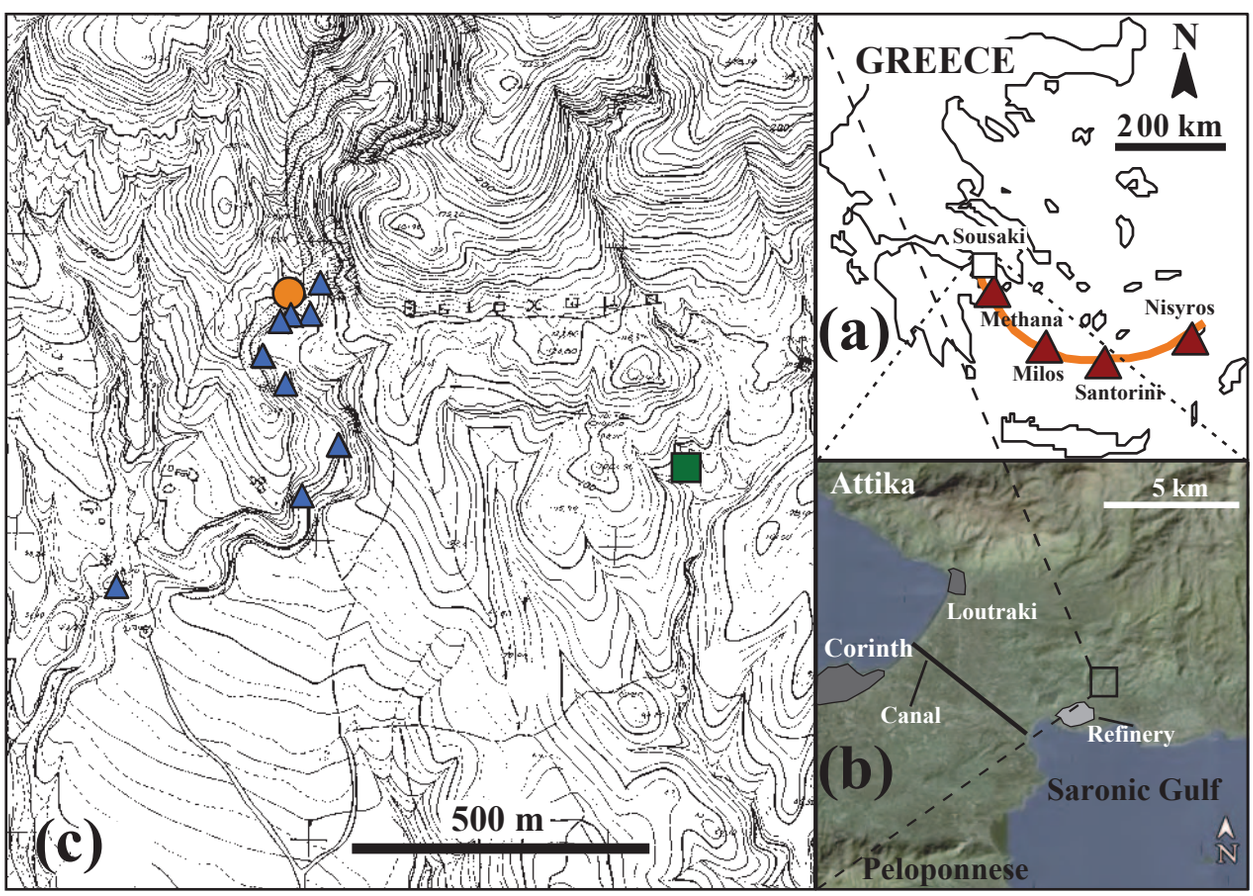
GREECE
N
200 km
Sousaki
Methana
Nisyros
Milos
Santorini
(a)
Attika
5 km
Loutraki
Corinth
Canal
Refinery
(b)
Saronic Gulf
N
Peloponnese
(c)
500 m

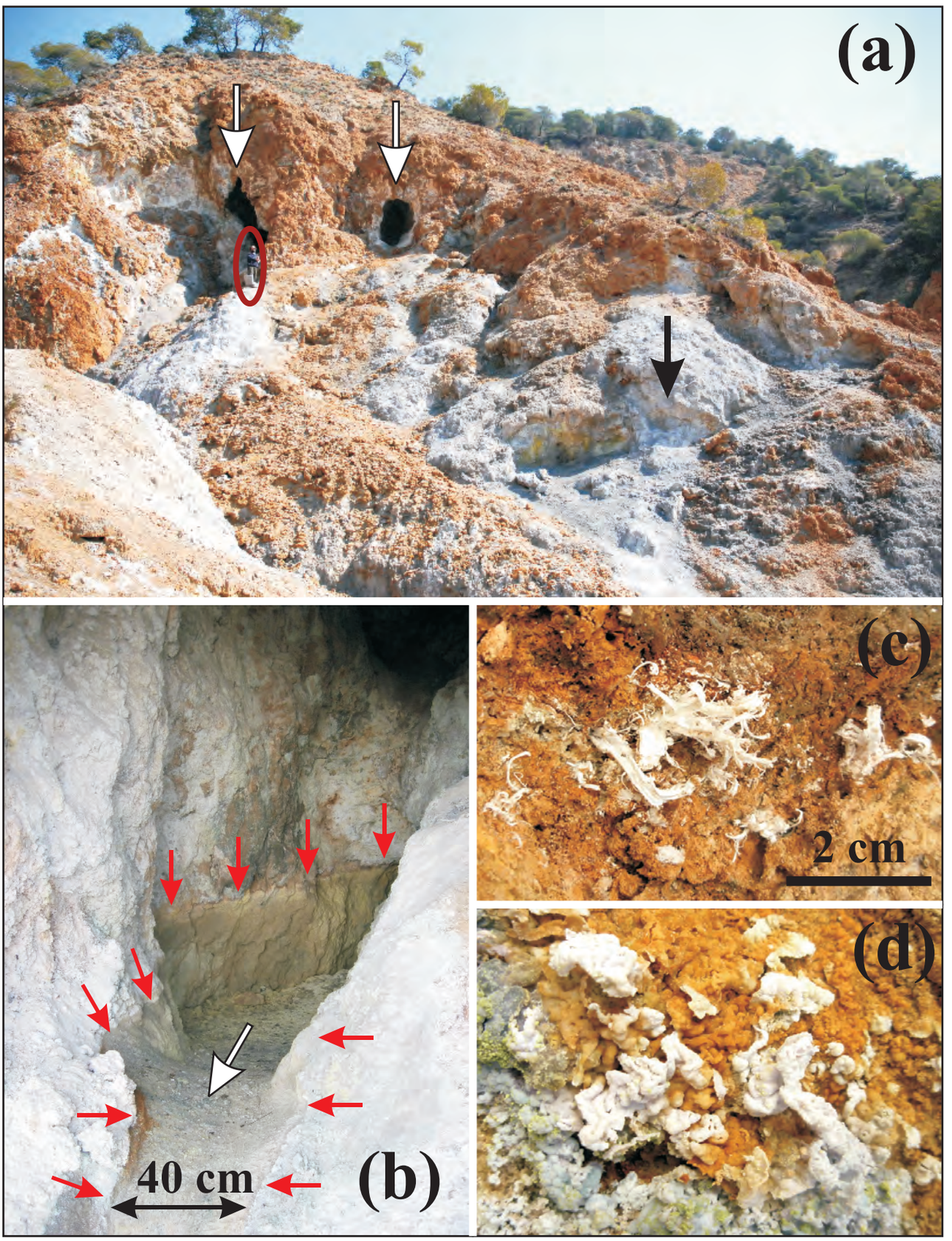
(a)
(b)
40 cm
(c)
2 cm
(d)

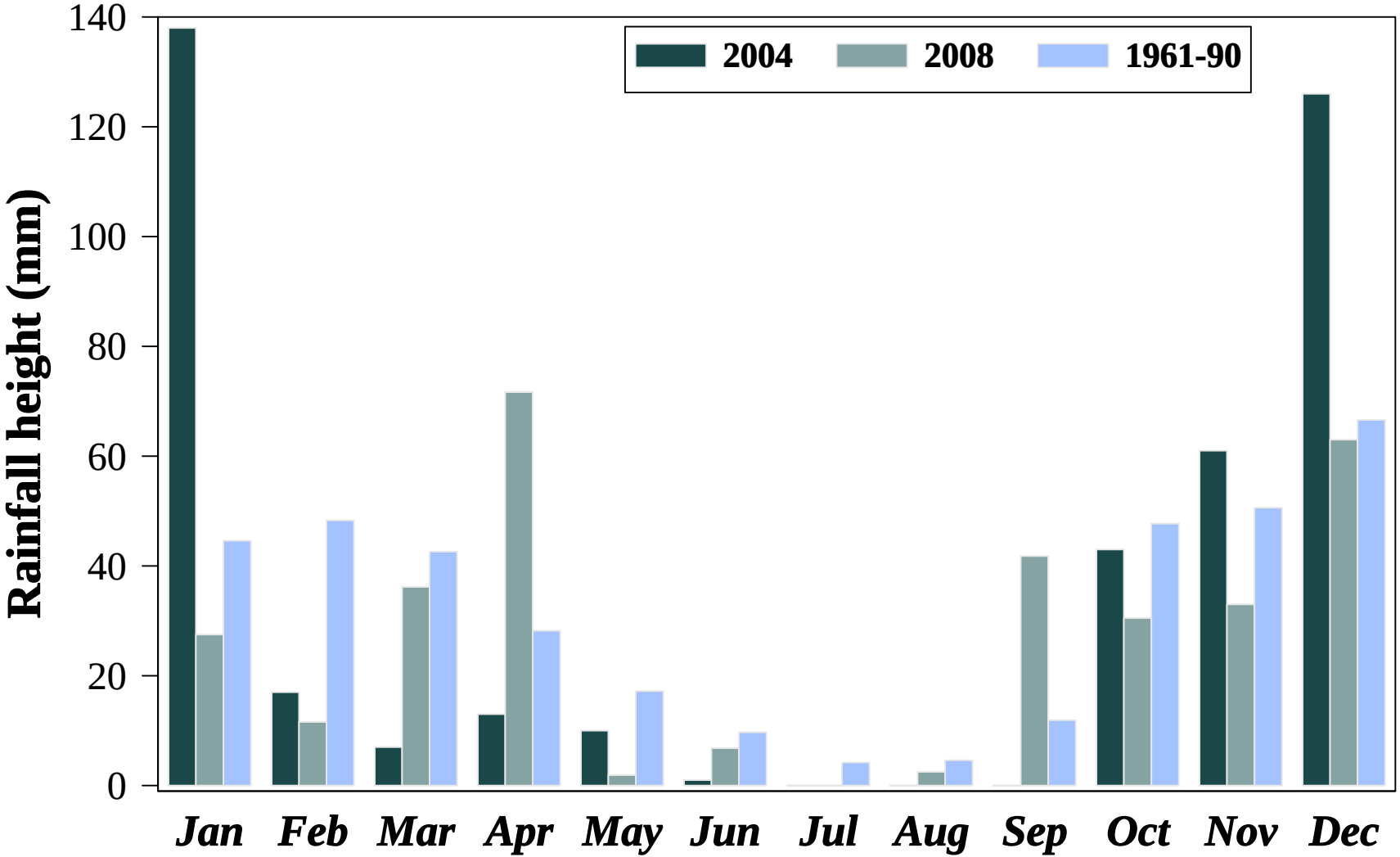
2004
2008
1961-90
Rainfall height (mm)
140
120
100
80
60
40
20
0
Jan
Feb
Mar
Apr
May
Jun
Jul
Aug
Sep
Oct
Nov
Dec

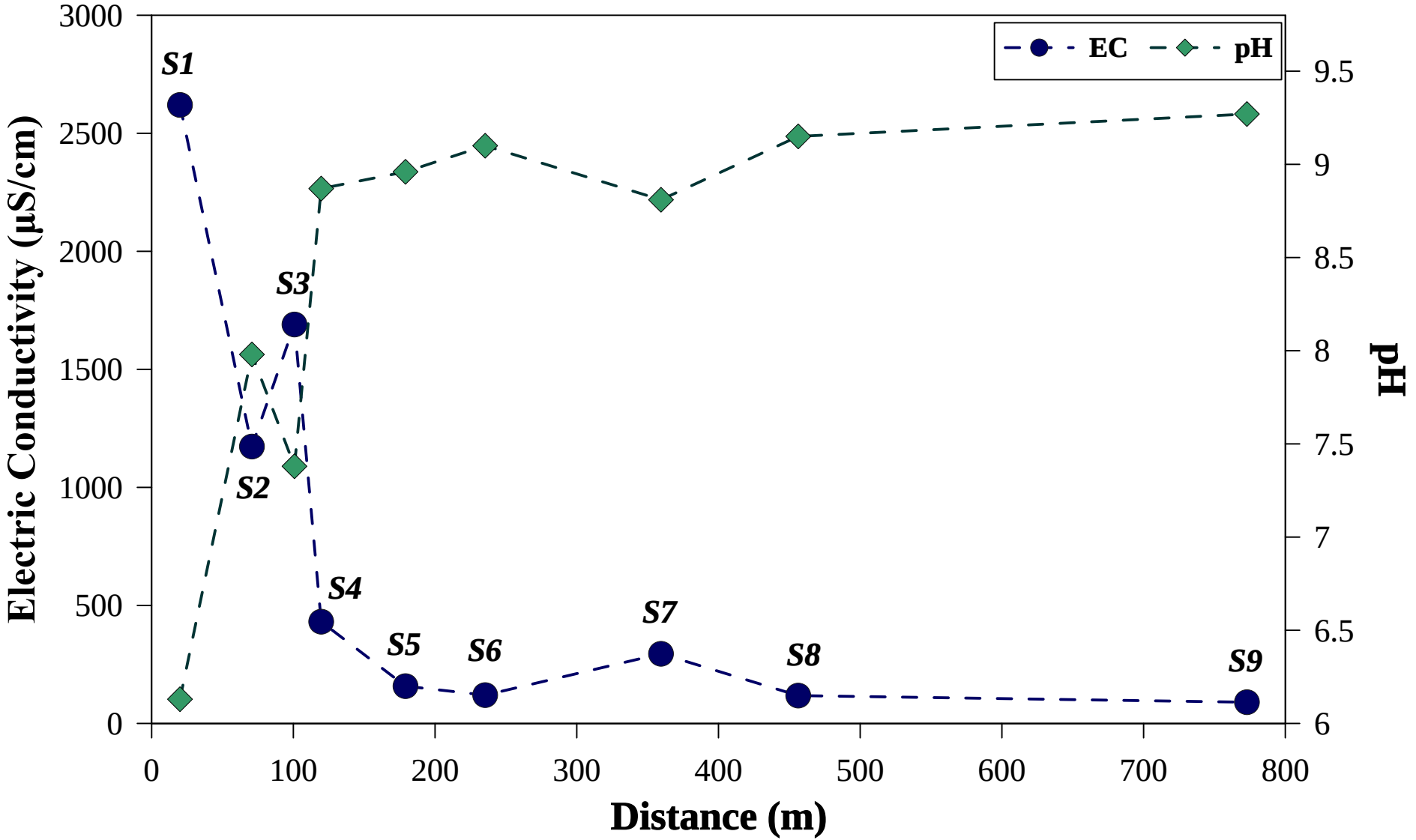
EC
pH
S1
S2
S3
S4
S5
S6
S7
S8
S9
Electric Conductivity (µS/cm)
pH
Distance (m)
3000
2500
2000
1500
1000
500
0
9.5
9
8.5
8
7.5
7
6.5
6
0
100
200
300
400
500
600
700
800

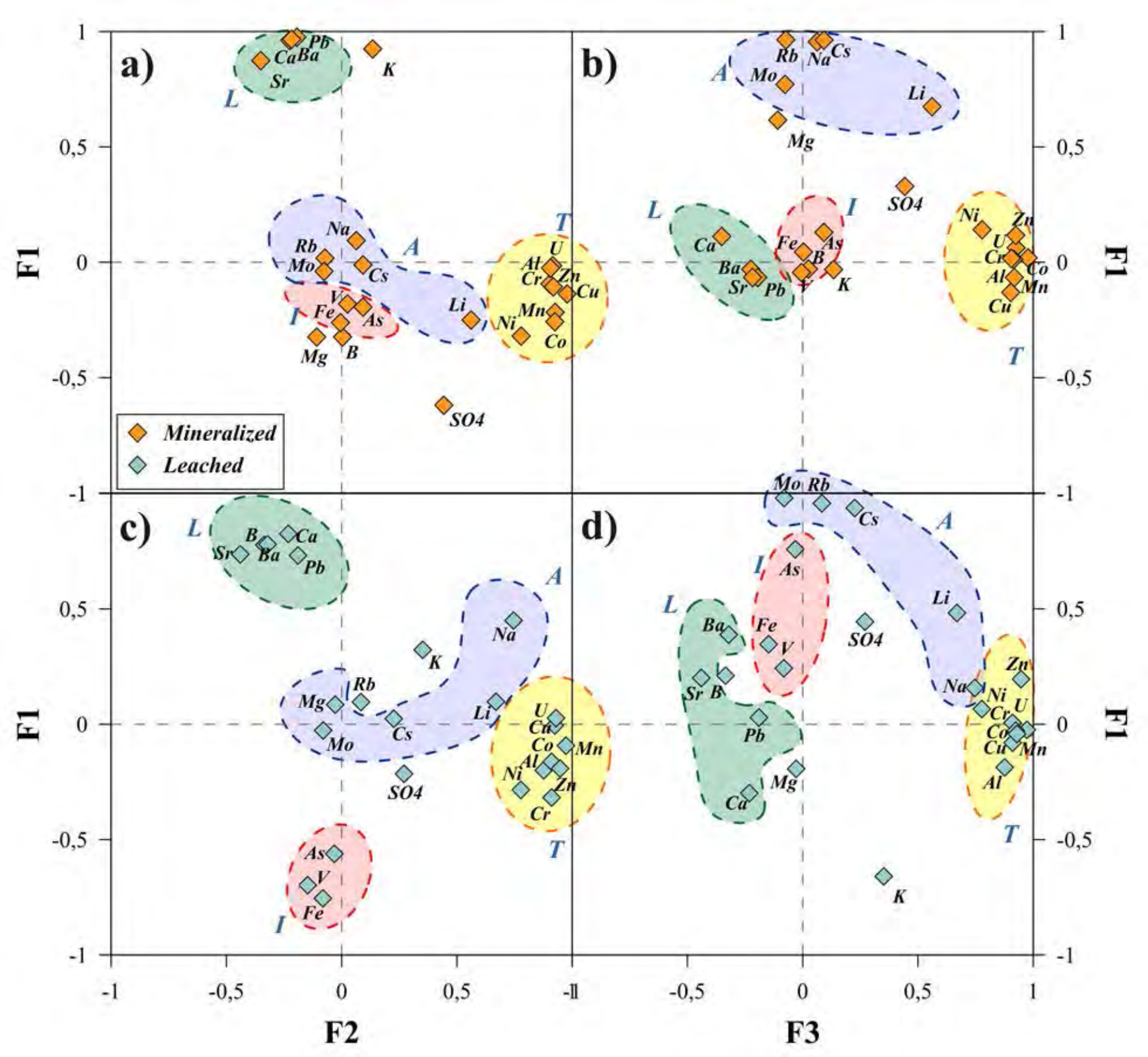
a)
b)
c)
d)
L
A
I
T
Mineralized
Leached
F1
F2
F3
Pb
Ca
Ba
Sr
K
Na
Rb
Mo
Cs
Li
V
Fe
As
Mg
B
SO4
U
Al
Cr
Zn
Cu
Mn
Ni
Co

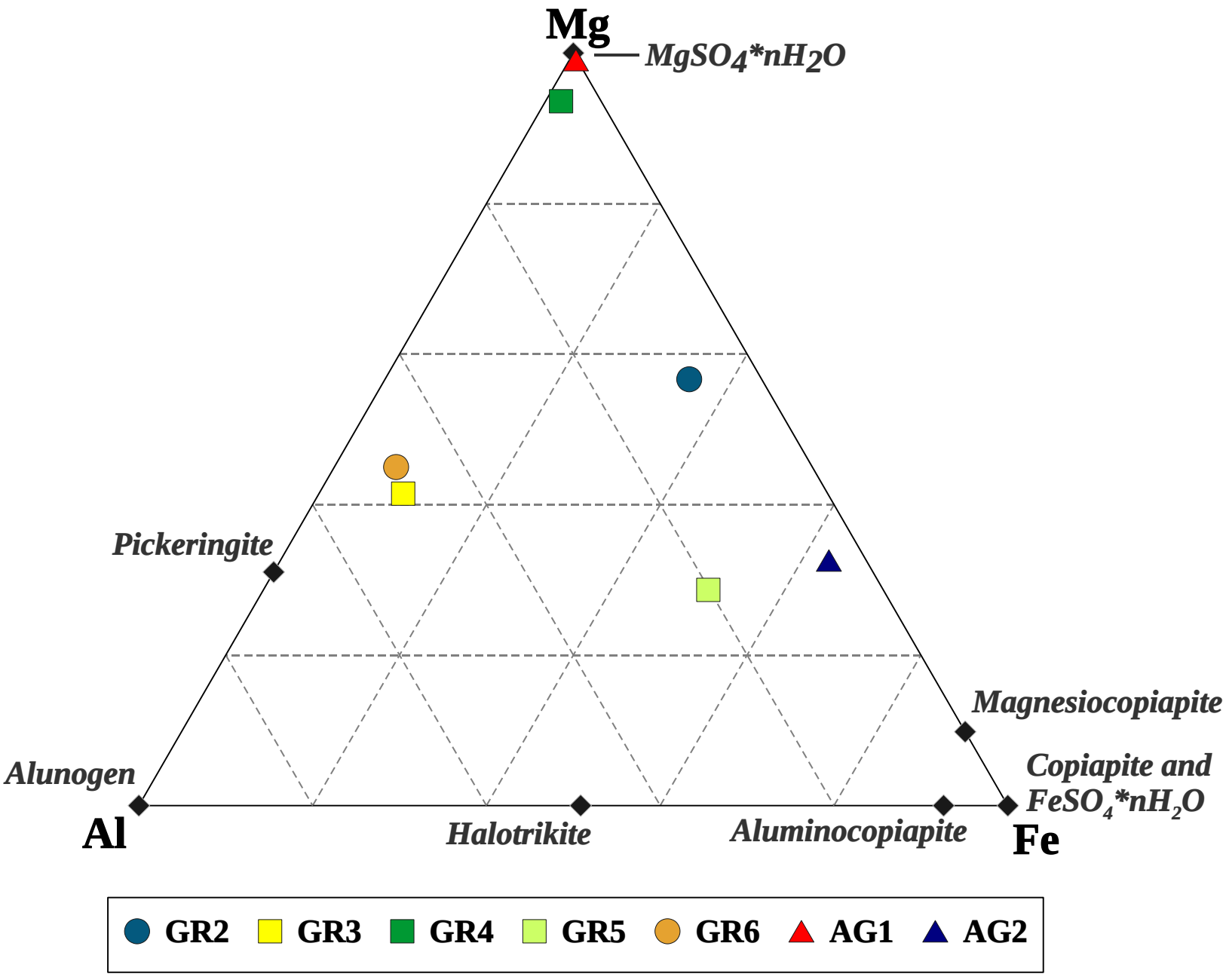
Mg
MgSO4*nH2O
Pickeringite
Alunogen
Al
Halotrikite
Aluminocopiapite
Magnesiocopiapite
Copiapite and
FeSO4*nH2O
Fe
GR2
GR3
GR4
GR5
GR6
AG1
AG2

Table 1. Results of the XRD analysis

Sample	Mineral phases
AL1	Gypsum
GR1	Native Sulfur
GR2	Kieserite, Anhydrite
GR3	Anhydrite, Cristobalite, Alunogen
GR4	Anhydrite, Hexahydrite, Wairakite
GR5	Magnesiocopiapite
AG1	Epsomite, Gypsum
AG2	Hexahydrite, Gypsum, Magnesiocopiapite
S1	Gypsum, Clay minerals, Quartz
S9	Calcite, Clay minerals

Table 2 – Results of the chemical analyses of the efflorescences

Mineralization																							
	Li	B	Na	Mg	Al	K	Ca	V	Cr	Mn	Fe	Co	Ni	Cu	Zn	As	Rb	Sr	Mo	Cs	Ba	Pb	U	SO_4
	µg/g																							
AL1	0.53	2.97	723	895	641	50000	175000	2.72	122	4.92	901	1.36	19.0	0.62	4.64	10.5	2.85	198	0.43	2.01	117	15.3	0.03	399000
GR1	0.12	9.79	283	1310	60	12000	4120	0.11	7.19	5.20	177	1.39	30.8	1.16	21.8	3.58	0.02	1.80	0.20	0.01	1.02	1.44	< 0.02	476000
GR2	8.70	6.69	2040	134000	2510	17000	15600	3.86	319	439	16800	165	3390	13.1	38.8	119	16.6	59.0	1.53	9.98	1.52	0.79	0.82	946000
GR3	5.47	10.9	674	90500	3080	23200	25300	1.75	136	525	2680	144	2780	8.98	25.2	20.8	1.32	51.4	< 0.02	1.42	2.25	0.52	1.49	952000
GR4	2.19	4.76	632	52900	43000	26500	21200	2.55	2140	1070	10200	431	6940	27.9	61.9	16.0	0.81	27.5	0.19	1.20	2.06	0.27	1.43	926000
GR5	7.83	2.98	504	43600	22000	21500	3990	19.8	3680	937	99000	235	7230	16.7	41.9	680	2.88	4.59	1.07	3.72	0.01	0.01	1.47	919000
GR6	8.92	6.55	788	40500	40700	25100	1580	2.67	5490	2740	6480	488	6550	180	87.2	43.1	2.34	10.9	0.30	3.09	0.29	0.41	12.7	982000
AG1	3.03	1.95	571	147000	244	22700	20100	0.83	37.4	154	1220	60.4	2170	2.28	6.35	8.12	0.43	80.2	0.16	0.67	1.80	0.35	0.11	914000
AG2	0.95	2.28	145	1180	5610	10200	479	18.6	1510	519	101000	141	2850	5.90	25.9	230	1.77	34.9	0.73	1.94	0.49	0.13	0.29	926000

Leaching																							
	Li	B	Na	Mg	Al	K	Ca	V	Cr	Mn	Fe	Co	Ni	Cu	Zn	As	Rb	Sr	Mo	Cs	Ba	Pb	U	SO_4
	µg/g																							
AL1	0.14	1.72	320	422	34.1	10800	42000	0.03	4.74	1.08	28.4	0.38	5.34	0.60	1.46	0.40	0.24	98.8	0.16	0.17	1.33	3.18	0.01	99600
GR1	0.09	0.68	169	121	51.6	6320	663	0.06	6.08	4.73	155	1.33	30.6	0.06	4.71	1.10	0.16	1.82	< 0.03	0.11	0.08	0.34	< 0.03	13000
GR2	9.88	0.97	439	26700	3930	3140	2630	3.99	281	421	16500	149	3340	12.1	35.9	86.6	18.6	59.8	1.17	11.4	1.09	0.67	0.85	620000
GR3	7.42	0.71	579	113000	5570	12300	34200	0.20	137	625	2160	164	3420	9.16	18.3	1.47	1.56	67.8	< 0.05	1.60	0.63	0.29	1.79	515000
GR4	1.70	0.24	237	35300	41600	10900	13900	1.80	1635	800	8250	333	5480	18.5	42.6	10.7	0.67	23.5	< 0.06	0.87	0.59	0.12	1.03	489000
GR5	7.87	< 0.04	403	34600	24300	10800	2640	4.04	2952	753	61800	197	6220	13.1	34.4	53.3	2.75	4.67	< 0.04	3.53	< 0.04	0.02	1.24	458000
GR6	10.1	< 0.04	669	44800	47700	9890	2900	2.04	5144	2530	7080	447	6220	179	81.0	21.6	2.58	12.4	0.15	3.25	0.10	0.40	12.8	476000
AG1	2.82	< 0.04	236	113000	195	6470	12300	0.08	20.6	137	872	52.9	2020	1.87	5.35	1.23	0.35	65.2	< 0.04	0.50	0.53	0.21	0.09	547000
AG2	0.92	< 0.04	114	40600	5370	6100	805	16.9	1174	386	78700	119	2360	5.14	21.6	99.6	1.60	36.6	0.51	1.63	0.22	0.04	0.25	508000

Se, Cd, Sb, Hg and Th were always below detection limit.

Table 3 – Factor analysis

mineralized	F1	F2	F3	F4
Li	0.562	-0.250	0.675	0.069
B	0.004	-0.324	0.045	-0.634
Na	0.063	0.095	0.956	-0.241
Mg	-0.108	-0.324	0.616	-0.334
Al	0.903	-0.094	-0.130	0.080
K	0.135	0.925	-0.031	-0.128
Ca	-0.225	0.962	-0.030	-0.076
V	0.026	-0.180	-0.029	0.966
Cr	0.919	-0.106	-0.066	0.337
Mn	0.978	-0.137	0.020	-0.004
Fe	-0.005	-0.261	-0.044	0.948
Co	0.926	-0.217	0.063	0.029
Ni	0.779	-0.320	0.142	0.345
Cu	0.916	-0.015	0.013	-0.183
Zn	0.925	-0.258	0.117	-0.015
As	0.093	-0.194	0.130	0.886
Rb	-0.072	0.018	0.965	0.037
Sr	-0.350	0.874	0.112	-0.118
Mo	-0.076	-0.039	0.772	0.571
Cs	0.093	-0.011	0.963	0.169
Ba	-0.194	0.976	-0.065	0.001
Pb	-0.217	0.967	-0.065	-0.038
U	0.906	-0.025	0.017	-0.189
SO_4	0.443	-0.620	0.329	0.146

leached	F1	F2	F3	F4
Li	0.669	0.098	0.483	0.410
B	-0.335	0.777	0.211	-0.440
Na	0.746	0.450	0.157	0.290
Mg	-0.028	0.085	-0.193	0.938
Al	0.876	-0.200	-0.187	0.014
K	0.351	0.323	-0.659	0.141
Ca	-0.231	0.826	-0.299	0.098
V	-0.148	-0.697	0.347	-0.029
Cr	0.911	-0.318	-0.080	-0.056
Mn	0.973	-0.093	-0.024	0.086
Fe	-0.082	-0.755	0.243	0.028
Co	0.911	-0.163	0.006	0.204
Ni	0.777	-0.285	0.066	0.396
Cu	0.925	-0.005	-0.028	-0.082
Zn	0.947	-0.192	0.196	0.057
As	-0.032	-0.561	0.758	-0.001
Rb	0.084	0.096	0.957	0.065
Sr	-0.440	0.737	0.201	0.190
Mo	-0.080	-0.027	0.981	-0.072
Cs	0.226	0.024	0.937	0.106
Ba	-0.321	0.780	0.389	-0.049
Pb	-0.190	0.731	0.029	-0.519
U	0.929	0.027	-0.042	-0.028
SO_4	0.270	-0.215	0.444	0.783

Table 4 – Physico-chemical parameters measured in the leachate solutions of the sediment samples and results of the chemical analyses

Sample	distance	pH	E.C.	Li	B	Na	Mg	Al	K	Ca	V	Cr	Mn	Fe	Co	Ni	Cu	Zn	As	Rb	Sr	Mo	Cs	Ba	Pb	U	SO_4
	m		µS/cm	µg/g																							
S1	0	6.13	2620	0.65	0.76	168	40500	0.09	174	22200	0.01	0.15	197	79.0	8.10	195	0.07	0.83	0.06	0.26	40.7	0.04	0.01	0.89	<0.01	<0.01	193000
S2	51	7.98	1173	0.12	0.50	21.6	649	0.22	57.5	22400	0.01	0.03	31.4	0.43	0.17	1.89	0.08	0.31	0.49	0.22	33.4	0.13	0.02	0.59	0.01	<0.01	54000
S3	81	7.38	1690	0.61	0.74	30.0	12100	1.10	37.2	24500	0.01	0.01	111	0.35	1.62	47.0	0.01	0.35	0.10	0.20	50.4	0.09	0.01	0.61	<0.01	0.02	106000
S4	100	8.87	431	0.54	0.75	232	846	0.86	153	6260	0.05	<0.01	3.47	0.62	0.04	0.97	0.04	<0.01	0.26	0.67	16.1	0.06	0.07	0.54	<0.01	<0.01	17100
S5	159	8.96	158	0.23	0.35	37.6	189	2.34	96.5	1600	0.09	0.02	0.37	1.36	0.00	0.11	0.05	0.43	0.27	0.42	3.9	0.05	0.04	0.49	<0.01	<0.01	3870
S6	215	9.10	120	0.13	0.33	36.4	201	1.35	85.2	1460	0.14	0.01	0.11	1.32	0.00	0.06	0.04	0.01	0.15	0.27	3.8	0.05	0.02	0.37	<0.01	<0.01	3500
S7	339	8.81	295	0.08	0.23	11.0	381	0.20	75.0	4250	0.06	0.01	1.10	0.35	0.01	0.18	0.02	0.05	0.35	0.18	6.6	0.05	0.01	0.41	<0.01	<0.01	10900
S8	436	9.15	118	0.18	0.33	40.2	126	4.57	96.7	858	0.14	0.01	0.13	2.71	0.00	0.11	0.05	<0.01	0.26	0.31	2.3	0.04	0.02	0.46	<0.01	<0.01	141
S9	753	9.27	90	0.24	0.82	54.7	170	11.1	217	677	0.41	0.07	0.24	16.5	0.02	0.54	0.23	<0.01	0.52	0.33	2.0	0.04	0.03	0.47	0.01	0.01	944

distance = progressive distance from the first sampling site along the creek. E.C. = Electric Conductivity. Se, Cd, Sb, Hg and Th were always below detection limit.

Declaration of interests

☒ The authors declare that they have no known competing financial interests or personal relationships that could have appeared to influence the work reported in this paper.

☐The authors declare the following financial interests/personal relationships which may be considered as potential competing interests: